Fluorescent porous silicon biological probes with high quantum efficiency and stability

Chang-Ching Tu,[1*] Ying-Nien Chou,[2] Hsiang-Chieh Hung,[2] Jingda Wu,[3] Shaoyi Jiang,[2] and Lih Y. Lin[3]

[1]*LumiSands, Inc., Seattle, WA, 98105, USA*
[2]*Department of Chemical Engineering, University of Washington, Seattle, WA, 98195, USA*
[3]*Department of Electrical Engineering, University of Washington, Seattle, WA, 98195, USA*
[*]*tucc@lumisands.com*

Abstract: We demonstrate porous silicon biological probes as a stable and non-toxic alternative to organic dyes or cadmium-containing quantum dots for imaging and sensing applications. The fluorescent silicon quantum dots which are embedded on the porous silicon surface are passivated with carboxyl-terminated ligands through stable Si–C covalent bonds. The porous silicon bio-probes have shown photoluminescence quantum yield around 50% under near-UV excitation, with high photochemical and thermal stability. The bio-probes can be efficiently conjugated with antibodies, which is confirmed by a standard enzyme-linked immunosorbent assay (ELISA) method.

OCIS codes: (160.2540) Fluorescent and luminescent materials; (160.4236) Nanomaterials; (250.5230) Photoluminescence.

References and links

1. A. Miyawaki, "Visualization of the spatial and temporal dynamics of intracellular signaling," Dev. Cell **4**(3), 295–305 (2003).
2. I. L. Medintz, A. R. Clapp, H. Mattoussi, E. R. Goldman, B. Fisher, and J. M. Mauro, "Self-assembled nanoscale biosensors based on quantum dot FRET donors," Nat. Mater. **2**(9), 630–638 (2003).
3. M. Veiseh, P. Gabikian, S.-B. Bahrami, O. Veiseh, M. Zhang, R. C. Hackman, A. C. Ravanpay, M. R. Stroud, Y. Kusuma, S. J. Hansen, D. Kwok, N. M. Munoz, R. W. Sze, W. M. Grady, N. M. Greenberg, R. G. Ellenbogen, and J. M. Olson, "Tumor paint: a chlorotoxin:Cy5.5 bioconjugate for intraoperative visualization of cancer foci," Cancer Res. **67**(14), 6882–6888 (2007).
4. U. Resch-Genger, M. Grabolle, S. Cavaliere-Jaricot, R. Nitschke, and T. Nann, "Quantum dots versus organic dyes as fluorescent labels," Nat. Methods **5**(9), 763–775 (2008).
5. I. L. Medintz, H. T. Uyeda, E. R. Goldman, and H. Mattoussi, "Quantum dot bioconjugates for imaging, labelling and sensing," Nat. Mater. **4**(6), 435–446 (2005).
6. L. Ye, K.-T. Yong, L. Liu, I. Roy, R. Hu, J. Zhu, H. Cai, W.-C. Law, J. Liu, K. Wang, J. Liu, Y. Liu, Y. Hu, X. Zhang, M. T. Swihart, and P. N. Prasad, "A pilot study in non-human primates shows no adverse response to intravenous injection of quantum dots," Nat. Nanotechnol. **7**(7), 453–458 (2012).
7. A. B. Sieval, A. L. Demirel, J. W. M. Nissink, M. R. Linford, J. H. van der Maas, W. H. de Jeu, H. Zuilhof, and E. J. R. Sudhölter, "Highly stable Si-C linked functionalized monolayers on the silicon (100) surface," Langmuir **14**(7), 1759–1768 (1998).
8. J. P. Proot, C. Delerue, and G. Allan, "Electronic structure and optical properties of silicon crystallites: Application to porous silicon," Appl. Phys. Lett. **61**(16), 1948–1950 (1992).
9. K. Dohnalova, A. N. Poddubny, A. A. Prokofiev, W. D. de Boer, C. P. Umesh, J. M. J. Paulusse, H. Zuilhof, and T. Gregorkiewicz, "Surface brightens up Si quantum dots: direct bandgap-like size-tunable emission," Light: Science and Technology **2**, e47 (2013).
10. C.-C. Tu, J. H. Hoo, K. F. Böhringer, L. Y. Lin, and G. Cao, "Red-emitting silicon quantum dot phosphors in warm white LEDs with excellent color rendering," Opt. Express **22**(S2), A276–A281 (2014).
11. J. M. Buriak, "Organometallic chemistry on silicon and germanium surfaces," Chem. Rev. **102**(5), 1271–1308 (2002).
12. J.-H. Park, L. Gu, G. von Maltzahn, E. Ruoslahti, S. N. Bhatia, and M. J. Sailor, "Biodegradable luminescent porous silicon nanoparticles for *in vivo* applications," Nat. Mater. **8**(4), 331–336 (2009).
13. Z. F. Li and E. Ruckenstein, "Water-soluble poly(acrylic acid) grafted luminescent silicon nanoparticles and their use as fluorescent biological staining labels," Nano Lett. **4**(8), 1463–1467 (2004).

14. J. H. Warner, A. Hoshino, K. Yamamoto, and R. D. Tilley, "Water-soluble photoluminescent silicon quantum dots," Angew. Chem. Int. Ed. Engl. **44**(29), 4550–4554 (2005).
15. F. Erogbogbo, K.-T. Yong, I. Roy, G. Xu, P. N. Prasad, and M. T. Swihart, "Biocompatible luminescent silicon quantum dots for imaging of cancer cells," ACS Nano **2**(5), 873–878 (2008).
16. F. Erogbogbo, C. A. Tien, C. W. Chang, K. T. Yong, W. C. Law, H. Ding, I. Roy, M. T. Swihart, and P. N. Prasad, "Bioconjugation of luminescent silicon quantum dots for selective uptake by cancer cells," Bioconjug. Chem. **22**(6), 1081–1088 (2011).
17. K. Fujioka, M. Hiruoka, K. Sato, N. Manabe, R. Miyasaka, S. Hanada, A. Hoshino, R. D. Tilley, Y. Manome, K. Hirakuri, and K. Yamamoto, "Luminescent passive-oxidized silicon quantum dots as biological staining labels and their cytotoxicity effects at high concentration," Nanotechnology **19**(41), 415102 (2008).
18. X. Cheng, S. B. Lowe, P. J. Reece, and J. J. Gooding, "Colloidal silicon quantum dots: from preparation to the modification of self-assembled monolayers (SAMs) for bio-applications," Chem. Soc. Rev. **43**(8), 2680–2700 (2014).
19. B. Averboukh, R. Huber, K. W. Cheah, Y. R. Shen, G. G. Qin, Z. C. Ma, and W. H. Zong, "Luminescence studies of Si/SiO$_2$ superlattice," J. Appl. Phys. **92**(7), 3564–3568 (2002).
20. M. Sykora, L. Mangolini, R. D. Schaller, U. Kortshagen, D. Jurbergs, and V. I. Klimov, "Size-dependent intrinsic radiative decay rates of silicon nanocrystals at large confinement energies," Phys. Rev. Lett. **100**(6), 067401 (2008).
21. K. Dohnalová, K. Kůsová, and I. Pelant, "Time-resolved photoluminescence spectroscopy of the initial oxidation stage of small silicon nanocrystals," Appl. Phys. Lett. **94**(21), 211903 (2009).
22. J. Valenta, A. Fucikova, F. Vácha, F. Adamec, J. Humpolíčková, M. Hof, I. Pelant, K. Kůsová, K. Dohnalová, and J. Linnros, "Light-emission performance of silicon nanocrystals deduced from single quantum dot spectroscopy," Adv. Funct. Mater. **18**(18), 2666–2672 (2008).
23. Y. Zhao, C. Riemersma, F. Pietra, R. Koole, C. M. Donegá, and A. Meijerink, "High-temperature luminescence quenching of colloidal quantum dots," ACS Nano **6**(10), 9058–9067 (2012).
24. C.-J. Huang, N. D. Brault, Y. Li, Q. Yu, and S. Jiang, "Controlled hierarchical architecture in surface-initiated zwitterionic polymer brushes with structurally regulated functionalities," Adv. Mater. **24**(14), 1834–1837 (2012).

1. Introduction

Fluorescent probes or labels are extensively used in a variety of biological investigations, such as *in vivo* cellular imaging [1], *in vitro* protein sensing [2] or even intraoperative tumor visualization [3]. The traditional fluorophores are made of organic dyes, such as fluorescein and cyanines, which have good enough photoluminescence quantum yield (PLQY) and well-established protocols for bio-conjugation, purification and optical characterization. However, their low photochemical and thermal stability sometimes limit their effectiveness in high illumination flux applications [4]. On the other hand, semiconductor quantum dots, such as CdS, CdSe, CdTe quantum dots, have emerged as promising substitutes for the organic dyes. They possess unique optical properties which make them stand out in some biological applications, including size-dependent photoluminescence (PL), high PLQY, narrow emission spectra (full-width at half-maximum, FWHM < 50 nm), broad excitation spectra, large stokes shift and high resistance to photobleaching [5]. However, their heavy-metal contents are potentially hazardous. Although capping with ZnS shells may prevent cadmium-leakage and minimize acute toxicity, the long-lasting process of *in vivo* quantum dot breakdown and clearance of heavy-metal is still under investigation and may cause concerns for potential clinical applications [6].

In this paper, we demonstrate porous silicon (PS) bio-probes which are much more stable than conventional organic dyes and do not contain any heavy-metal like CdSe quantum dots. The fluorescent silicon quantum dots (SiQDs) which are embedded on the PS particle surface are passivated with stable Si–C covalent bonds. The entire PS bio-probe surfaces are terminated with carboxyl groups which make them ideal for bio-conjugation through a standard *N*-hydroxysuccinimide/ethyl(dimethylaminopropyl) carbodiimide (NHS/EDC) procedure. The red-emitting PS bio-probe suspensions in water have shown PLQY around 50% under near-UV excitation, with high photochemical and thermal stability. The PS bio-probes can also be self-assembled on a planar surface through ionic attractions, and imaged by a conventional fluorescent microscope. Finally, the loading of antibodies on the bio-probe surfaces was verified by an enzyme-linked immunosorbent assay (ELISA) method.

2. Experiment

The synthesis process of the PS bio-probes is illustrated in Fig. 1(a) to 1(e). Firstly, a 6-inch p-type silicon wafer with (100) orientation and 5 ~20 Ω-cm was electrochemically etched at a constant current density of 2.8 mA / cm^2 in the electrolyte comprising 48% HF: methanol = 13: 22 (volume ratio), creating a micron-sized porous silicon layer in which SiQDs are embedded on the surface [Fig. 1(a)]. Secondly, the silicon wafer was treated with diluted HF and subsequently immersed in pure deoxygenated 10-undecylenic acid (UDA) methyl ester for a hydrosilylation reaction at 200°C for 20 hours. The hydride groups (Si–H) on the silicon surface react with the vinyl groups (–CH = CH$_2$) of the UDA to form Si–C covalent bonds [Fig. 1(b)]. Note that the methyl ester can be converted back to carboxyl group by hydrolysis at the end of the synthesis process [7]. The porous silicon layer was mechanically removed from the wafer surface, sonicated, and then dispersed in a mixture of HNO$_3$ and HF for a "selective-etching" reaction. The Si–C passivation protects the SiQDs from being etched, while the bare silicon surface that was connected to the wafer is exposed for etching [Fig. 1(c)]. After the selective-etching, the micron-sized silicon core was greatly reduced in size, while almost all SiQDs were preserved [Fig. 1(d)]. Finally, the resulting PS particles were refluxed in 11-mercaptoundecanoic acid (MUA) solution in butanol at ~150°C, for capping the rest of the particle surface with carboxyl groups [Fig. 1(e)]. With the high temperature and the presence of acid as catalyst, the thiol group (–SH) of MUA might be capable of a nucleophilic attack to the silicon atom of Si–OH or Si–O–Si bonds at the PS particle surface, and the Si–S bonds can be likely formed. Alternatively, the MUA ligands might be simply physisorbed on the oxidized silicon surface. Experimentally, the increase of solubility of PS particles in water after reflux with MUA was clearly and consistently observed. In general, about 30 mg of PS bio-probes was obtained per wafer per synthesis, and the concentration of about 0.5 ~1 mg / mL in water was used for all optical characterizations. The PS bio-probe diameters were characterized using a Horiba Partica laser scattering particle size distribution analyzer (LA-950V2). The PL and excitation spectra were measured using a Jobin Yvon Horiba Fluorolog FL-3 fluorometer system. The PLQYs were measured using a Hamamatsu External Quantum Efficiency Measurement System (C9920). The ATR-FTIR spectra were recorded using a Shimadzu IRPrestige-21 system. The PL lifetimes were measured using a PicoQuant Time-Correlated Single Photon Counting System.
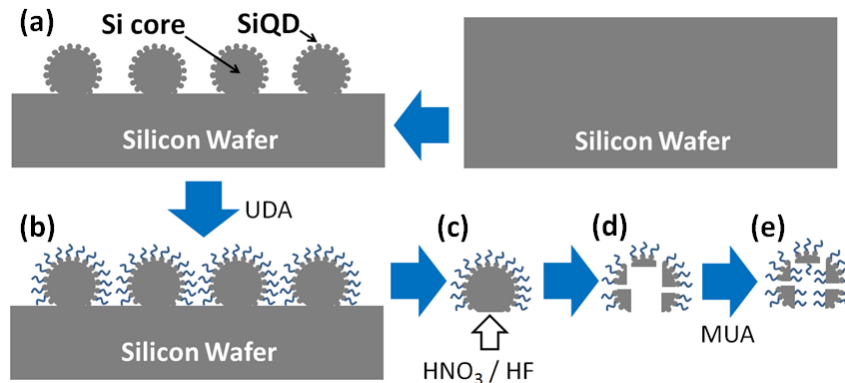

Fig. 1. (a)-(e) Illustration of the synthesis process of the PS bio-probes.

3. Results and discussion

The structure of PS bio-probes is composed of a micron-sized silicon core with nano-sized SiQDs embedded on its surface. A comparison of the particle size distribution of the PS bio-probes with (blue-line) and without (red-line) the selective-etching step is shown in Fig. 2(a).

By using the selective-etching technique, the majority core sizes were decreased from original 5 ~10 μm to 1 ~3 μm, and the proportion of nano-sized cores was greatly increased. The TEM images of the silicon core surface are shown in Fig. 2(b) and 2(c), on which the clusters of SiQDs can be observed. The SiQDs are of sizes ≤ 4 nm, which are smaller than the Bohr exciton radius of bulk silicon (~4.9 nm), enabling the quantum confinement effect [8] and the "quasi-direct bandgap" for efficient PL [9]. The photographs of the PS bio-probe suspension in water under room light and 365-nm excitation are shown in Fig. 2(d). Noticeably, the suspension appeared much clearer than our previous samples [10], because of its smaller particle sizes and enhanced solubility in water.

Theoretically, the selective-etching technique can remove the entire silicon cores, leaving only the SiQDs, as long as all SiQD surfaces are thoroughly protected by the Si–C bonds. However, in practice, the coverage of Si–C bonds can only reach up to about 50% of starting Si–H sites, due to the steric effects between ligands used for hydrosilylation [11]. In other words, the HNO_3 / HF etchant might also attack SiQDs during the selective-etching step, but with a much slower rate than etching the bare silicon surfaces of the cores. Experimentally, under a strong etching condition, the PL slowly moved from red to yellow, indicating the sizes of SiQDs becoming smaller due to the etching, as shown in Fig. 3(a). The Si–C protection can be further strengthened by using ligands of longer alkyl chains, whose hydrophobicity can expel the aqueous HNO_3 or HF molecules away from the SiQDs.
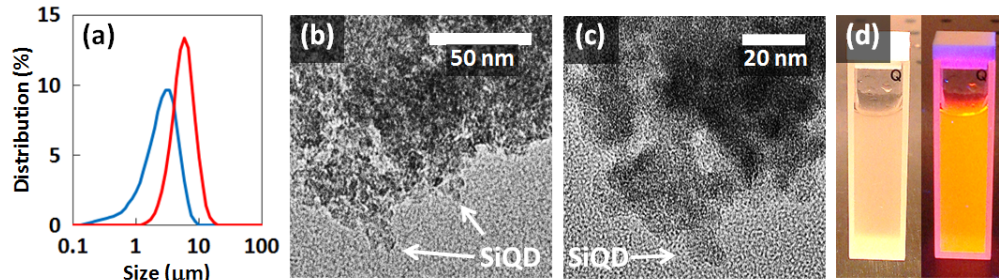

Fig. 2. (a) Particle size distribution of the PS bio-probe suspension in water, with (blue-line) and without (red-line) the "selective-etching" treatment. (b) and (c) TEM images of the PS bio-probes in low and high magnification, respectively. (d) Photographs of the PS bio-probe suspension in water under room light (left) and 365-nm excitation (right).

Noticeably, water-soluble porous silicon nanoparticles for bio-imaging have been previously reported [12]. In their work, sonication was applied to physically separate SiQDs from the cores, followed by filtration to remove the large particles. However, this approach usually wastes a lot of SiQDs, leading to low production yields and moderate PLQY (~10.2%). On the other hand, water-soluble free-standing SiQDs have been synthesized through various bottom-up routes, such as aerosol pyrolysis and precursor nucleation in solution, and bio-imaging applications based on these SiQDs have been demonstrated [13–18]. However, likely because the crystallinity of these SiQDs is not high enough, only moderate PLQY (10 ~30%) was reported. In contrast, in this work the PS bio-probes as a whole, including the cores and SiQDs, are all made of crystalline silicon, as they are harvested from the same single-crystalline silicon wafer. Their high crystallinity confirmed by high resolution TEM is one of the main factors contributing to the reported high PLQY here.

The spectral properties of the PS bio-probe suspension in water are shown in Fig. 3(a). The samples made with a weak, moderate and strong selective-etching condition have PL peak / FWHM = 642 nm / 128 nm, 627 nm / 130 nm and 600 nm / 102 nm, respectively (red-, orange- and green-curve). Specifically, the volume ratio of 70% HNO_3: 48% HF for the aforementioned weak, moderate and strong selective-etching condition = 400: 1, 40: 1, 20: 1, respectively. The suspension can be most efficiently excited in the range of 350 ~400 nm, whereas the absorption drops significantly in the range of 400 ~500 nm likely due to the

indirect bandgap nature of silicon, leading to low excitation efficiency in that range (blue-curve). The emission peak wavelengths, although not changing much, are almost linearly dependent on the excitation wavelengths, suggesting direct band-to-band recombination of photo-excited electron-hole pairs in the SiQDs (red-diamonds). The PS bio-probe suspension in water has PLQY = 53%, 47% and 42%, with 325-nm, 365-nm and 405-nm excitation, respectively, as shown in Fig. 3(b). For comparison, the red-emitting Cy5 organic dyes in phosphate buffered saline (PBS) have PLQY = 27% and the water-soluble red-emitting CdTe quantum dots have PLQY = 30 ~75% [4]. To achieve the high quantum yields, the step of reflux with MUA in butanol at a relatively high temperature (~150°C) plays the critical role. After the selective-etching step and before the reflux with MUA, the PLQY is around 20% with 365-nm excitation. Similar conclusions were reached in our previous work to obtain high PLQYs in non-polar solvents [10]. During the reflux, radiative oxide-related defect states, such as non-bridging oxygen-hole center (NBOHC) [19], are likely formed on the SiQD surface where the Si–C bonds are not covered. Besides, with the selective-etching technique, the non-radiative micron-size silicon cores are greatly reduced in size, minimizing the unfavorable PL re-absorption effect.
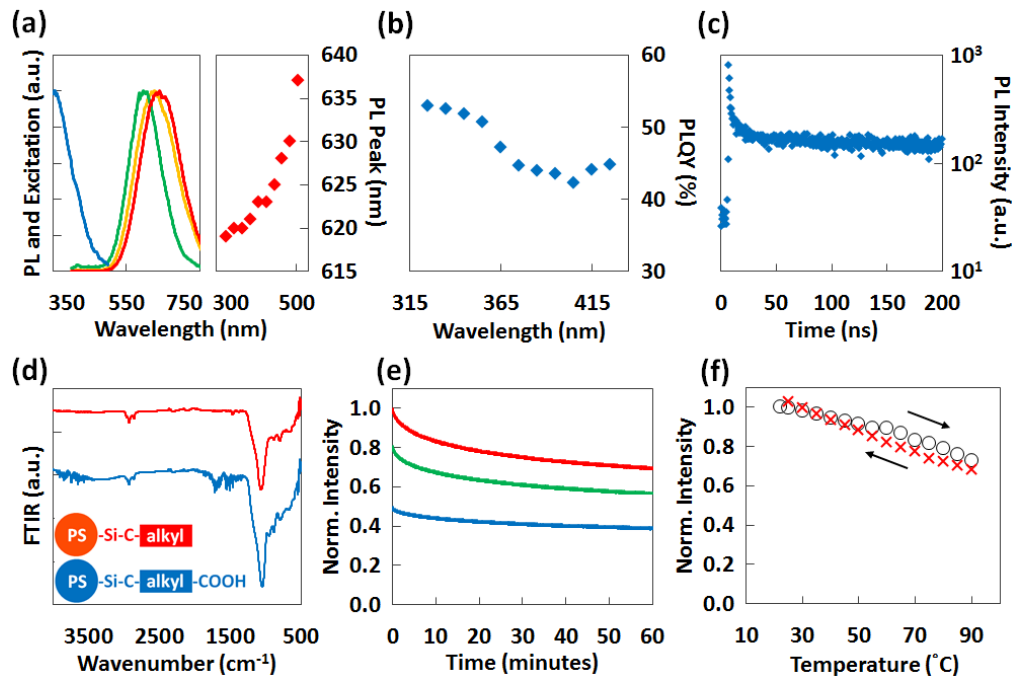

Fig. 3. (a) Center: PL spectra of the PS bio-probe suspension in water, made with a weak (red-curve), moderate (orange-ruve) and strong (green-curve) selective-etching condition. Left and Right: Excitation spectrum (blue-curve) and PL peak wavelength vs. excitation wavelength (red-diamonds) of the orange-curve sample. (b) and (c) PLQY vs. excitation wavelength and PL lifetime of the organge-curve sample in (a). (d) ATR-FTIR spectra of the PS bio-probe (blue-curve) and a reference PS sample passivated with pure alkyl chains (red-curve). (e) Time-resolved normalized PL intensity of the PS bio-probe suspension in water, under 405-nm high-power LED illumination with intensity = 2.8 mW / cm² (red-curve), 2.1 mW / cm² (green-curve) and 1.3 mW / cm² (blue-curve), respectively. (f) Temperature-resolved normalized PL intensity of the PS bio-probe suspension in water. (Black-circle: increasing temperature; red-cross: decreasing temperature).

The PL lifetime of the PS bio-probe suspension in water is shown in Fig. 3(c). The PL relaxation process has a fast component (τ ~5 ns) superimposed on a slow component ($\tau = 10$ ~100 µs). Similar PL dynamics were observed for SiQDs made from plasma dissociation of SiH$_4$ and also passivated with Si–C bonds like in this work [20]. In summary, upon photo-

excitation, an exciton (electron-hole pair) is created and then thermally relaxed to the lowest energy quantized state. From there, the exciton may have three possible recombination routes: Firstly, the exciton can recombine radiatively through a direct band-to-band transition, which corresponds to the fast component in Fig. 3(c). Secondly, the exciton can be trapped to oxide-related defect states on the SiQD surface and then recombine radiatively, which corresponds to the slow component in Fig. 3(c) [21]. Thirdly, the exciton may recombine through deep non-radiative recombination centers, which lowers the overall PLQY. The Si–C passivation on the SiQDs gives rise to their "quasi-direct bandgap" character and the fast, tunable PL. In contrast, the silicon oxide on the SiQDs may create radiative defect states which are responsible for the slow PL with limited spectral tunability [9]. As mentioned previously, since only up to about 50% of the Si–H sites on the SiQD surface are replaced by the Si–C bonds in the hydrosilylation reaction, the remaining sites tends to be easily oxidized into various silicon oxide forms, such as Si–O–Si, Si = O, Si–OH.

The attenuated total reflectance (ATR)-FTIR spectrum of the PS bio-probes is shown in Fig. 3(d). For comparison, a reference PS sample was synthesized and measured, by replacing the UDA and MUA with 1-decene and 1-dodecanethiol, respectively. The reference sample has surface chemistry almost identical to the PS bio-probes except no carboxyl termination at the ends of the alkyl chains, as illustrated in the inset of Fig. 3(d). Both the PS bio-probe (blue-line) and the reference sample (red-line) show absorption due to C–H$_x$ (2855, 2924 and 1458 cm^{-1}), Si–O–Si (950 ~1250 cm^{-1} and 793 cm^{-1}) and O–Si–H (878 cm^{-1}). Meanwhile, the PS bio-probe sample has additional absorption regions attributed to the carbonyl group (C = O, 1710 ~1720 cm^{-1}) and the hydroxyl group (–OH, 3000 ~4000 cm^{-1}), indicating that the PS bio-probes were successfully capped with carboxyl groups (–COOH) for their stable aqueous suspension and capability of bio-conjugation.

Here we measured the PL stability of the PS bio-probe suspension in water under high power LED illumination, as shown in Fig. 3(e). During the characterization, the suspension was placed in a close proximity to a 405-nm LED source, and a nearby silicon photodetector covered with a 590-nm longpass filter was used for measuring the red-emitting PL over time. Under constant illumination of intensity = 2.8, 2.1 and 1.3 mW / cm^2 (red-, green- and blue-curve), the suspension showed only 30%, 30% and 21% decrease of PL intensity in 1 hour, respectively. For comparison, conventional organic dyes usually have a photobleaching time less than 20 minutes, when used in a standard fluorescent imaging setting [13]. The light-induced degradation of the PS bio-probes likely results from a combination of the blinking effect [22], especially considering the slow component of the PL lifetime [Fig. 3(c)], and the formation of non-radiative defect states on the SiQD surfaces.

Here we also characterized the relative PL intensity of the PS bio-probe suspension in water at different temperatures, as shown in Fig. 3(f). The excitation source, a 365-nm high power LED, was on shortly only when we recorded the PL intensity readings at the specific temperatures, so that the light-induced degradation effect in Fig. 3(e) was excluded. Compared to 25°C, the suspension had about 30% decrease of PL intensity at 90°C, and the degradation was fully recoverable after sweeping back to room temperature. In contrast, conventional organic dyes, especially near-IR dyes, usually have poor thermal stabilities [4]. The recoverable thermal degradation of the PS bio-probes is likely related to thermally-created temporary trapping states or thermally-activated trapping processes through pre-existing defect states [23]. After the heat source is removed, the temporary trapping states or processes are eliminated accordingly, so that the PL intensity might return back to its original value at room temperature.

The PS bio-probes terminated with negatively-charged carboxyl groups can be self-assembled on a glass substrate coated with positively-charged polydiallyldimethylammonium chloride (PDDA) polymer through ionic attractions in water. The PS bio-probe monolayer can be clearly imaged by using a standard fluorescent microscope, as shown in Fig. 4(a), with excitation bandpass filter at 540 ~580 nm, dichromatic longpass mirror at 595 nm and

emission bandpass filter at 600 ~660 nm. Here we demonstrate the PS bio-probes can be further conjugated with horeseradish peroxidase (HRP)-modified goat anti-human IgG antibody through a standard NHS/EDC procedure, as illustrated in Fig. 4(b).
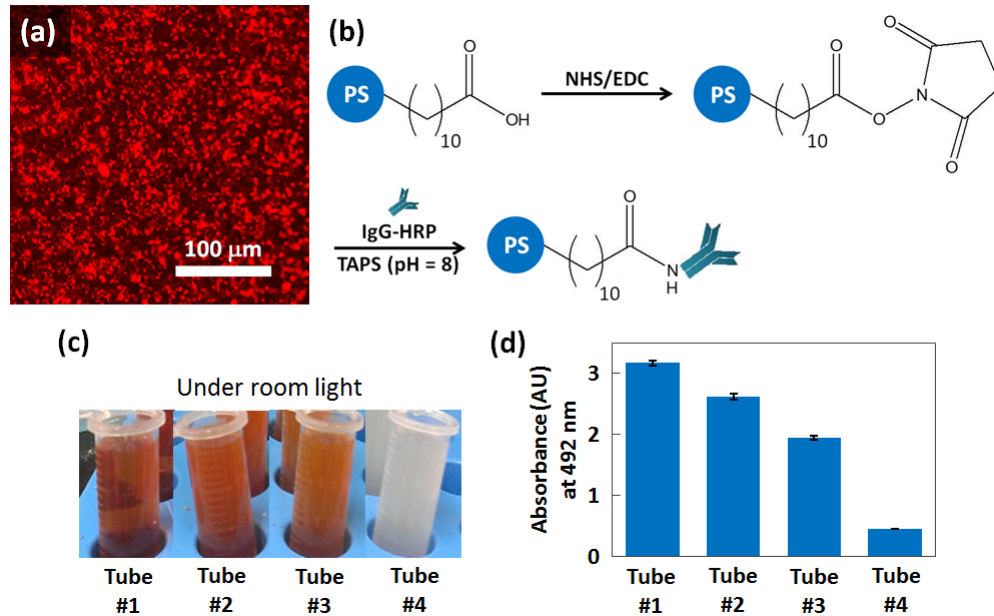

Fig. 4. (a) Fluorescent microscope image of the PS bio-probes assembled a glass slide coated with PDDA. (b) Illustration of the PS bio-probe conjugated with HRP-IgG though NHS/EDC. (c) and (d) After adding OPD, the photographs and the ELISA absorbance of Tube #1: HRP-IgG (0.1 μg / mL) in 1 mL PBS, Tube #2: PS bio-probes (0.5 mg / mL) in 1 mL PBS [activated by NHS/EDC and then incubated with HRP-IgG (0.1 μg / mL)], Tube #3: PS bio-probes (0.5 mg / mL) in 1 mL PBS [directly incubated with HRP-IgG (0.1 μg / mL)], and Tube #4: PS bio-probes (0.5 mg / mL) in 1 mL PBS as the blank

To verify the conjugation mechanism, an experiment was conducted as following. Tube #1: HRP-IgG (0.1 μg / mL) stored in 1 mL PBS. Tube #2: PS bio-probes (0.5 mg / mL) activated by NHS/EDC, incubated with HRP-IgG (0.1 μg / mL), washed away residual proteins and stored in 1 mL PBS. Tube #3: PS bio-probes (0.5 mg / mL) directly incubated with HRP-IgG (0.1 μg / mL), washed away residual proteins and stored in 1 mL PBS. Tube #4: PS bio-probes (0.5 mg / mL) stored in 1 mL PBS as the blank. Finally, each tube was added with o-phenylenediamine (OPD) as the HRP substrate. The solution with the presence of HRP would become orange-red under room light, as shown in Fig. 4(c). The absorbance at 492 nm, measured by an ELISA plate reader, is proportional to the HRP concentration. As shown in Fig. 4(d), about 80% and 55% of the original HRP-IgG antibodies (0.1 μg / mL) were loaded onto the PS bio-probes with and without NHS/EDC treatment, respectively. In other words, the HRP-IgG and PS bio-probe conjugation could happen even without NHS/EDC. In this case, the antibodies were physically absorbed onto the porous silicon which has a vast surface-area-to-volume ratio. Previously, PS nanoparticles were coated with dextran by a similar physical approach [12]. To avoid unwanted fouling and increase the conjugation selectivity, coating the PS bio-probes surfaces with a zwitterionic non-fouling layer is under investigation [24].

4. Conclusion

We demonstrate red-emitting PS bio-probes as a potential alternative to organic dyes or cadmium-based quantum dots for imaging and sensing applications. By using the selective-

etching technique, the ratio of nano-sized SiQDs to micron-sized silicon cores is greatly increased. The PS bio-probes are most efficiently excited in the near-UV range with PLQY ~50%. The SiQDs embedded on the PS surface are passivated with stable Si–C bonds, leading to their high photochemical and thermal stability. Furthermore, the entire PS bio-probe surfaces are terminated with carboxyl groups which facilitate bio-conjugation. The PS bio-probes can be self-assembled on a planar surface through ionic attractions and imaged by a standard fluorescent microscope. Finally, HRP-IgG antibodies can be efficiently loaded on the PS bio-probes through a common NHS/EDC procedure or simply by physical absorption.